# Finite Element Basis Functions for Nested Meshes of Non-Uniform Refinement Level

Volker HILL, Ortwin FARLE, and Romanus DYCZIJ-EDLINGER, *Member, IEEE*

***Abstract*— We propose a systematic methodology for the construction of hanging variables to connect finite elements of unequal refinement levels within a nested tetrahedral mesh. While conventional refinement schemes introduce irregular elements at such interfaces which must be removed when the mesh is further refined, the suggested approach keeps the discretization perfectly nested. Thanks to enhanced regularity, mesh-based methods such as refinement algorithms or intergrid transfer operators for use in multigrid solvers can be implemented in a much simpler fashion. The present paper covers $H^1$ and $H(curl)$ basis functions for triangular or tetrahedral elements.**

***Index Terms*— Electromagnetic fields, finite element methods, edge and facet elements.**

## I. Introduction

NESTED finite element (FE) meshes [1] - [6] possess a number of special properties that make them very well-suited for adaptive methods. First, they guarantee a lower bound on mesh quality when portions of the mesh are repeatedly refined [1] [2] [5]. Second, they are perfectly suited for geometric multigrid methods [1] [3] [4] [5] and hence allow for highly efficient linear equation solvers. Third, they exhibit a high degree of regularity which can be exploited in error estimators or for data extrapolation.

However, one difficulty with nested meshes is that, in case of non-uniform refinement, elements of unequal refinement levels must be connected without destroying the proper continuity of the basis functions across element interfaces. In conventional schemes, regions of unequal refinement levels are stitched together by means of so-called "red" and "green" elements [3] [4] [6]. Such elements are irregular in the sense that they are of inferior quality than their parents and ought to be removed when the mesh is further refined. Therefore, the sequence of FE spaces is no longer fully nested, and the construction of intergrid transfer operators becomes more complicated. Moreover, in the three-dimensional case, the number of possible element configurations to be taken into account is getting large. As a result, computer implementations of such methods tend to be rather complicated.

Alternatively, as shown in Fig. 1, one may allow elements of unequal refinement levels to touch, but impose suitable constraints on the basis functions to maintain the proper interface conditions along common edges or faces. Since the construction of such constraints is intimately related to that of intergrid transfer operators [5], this approach is particularly attractive in the context of multigrid solvers. Moreover, its computer implementation is rather straightforward.

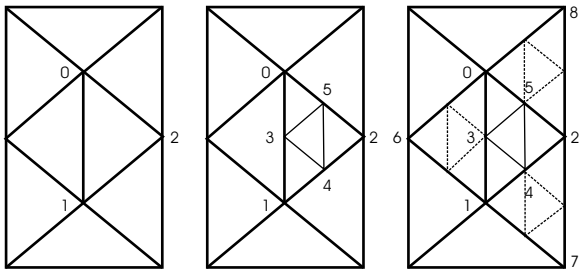


Fig. 1. a: Initial mesh. b: Basic refinement. c: Extended refinement.

In this paper, we develop two variants of the hanging variables approach and compare their respective properties with regard to flexibility, memory consumption, and numerical convergence.

## II. Hanging Variables

For simplicity, we describe the principle of hanging variables in two spatial dimensions. Given the consistent mesh of Fig. 1a, assume that triangle $T_{012}$ is to be refined. This leads to the situation depicted in Fig. 1b, featuring three hanging nodes, $\{N_3, N_4, N_5\}$, six hanging edges, $\{E_{03}, E_{31}, E_{14}, E_{42}, E_{25}, E_{50}\}$, plus three interior edges, $\{E_{34}, E_{45}, E_{53}\}$. The main idea to restore the proper interface conditions is to permit only such superpositions of fine mesh basis functions that their continuous components match their coarse mesh counterparts on the common interface. However, if we applied this method directly to the boundary $\{E_{01}, E_{12}, E_{20}\}$, we would create an unwanted restriction of the FE space in the interior. Specifically, for first order $H^1$ elements, all basis functions are associated with nodes, and all nodes of triangles $\{T_{035}, T_{143}, T_{425}, T_{345}\}$ lie on the outer boundary. By imposing continuity across the interface, we would just recover the FE space of the parent triangle $T_{012}$ and hence completely undo the refinement. To avoid such pitfalls, we refine all elements that share an edge with $T_{012}$ as in Fig. 1c and impose restrictions on the FE spaces associated with the triangle subdivisions in the so created buffer region. Such constraints must meet the following three requirements:

1) The basis functions of each buffer triangle subdivision must provide the proper continuity conditions across its interfaces to all adjacent refined or non-refined elements.
2) The FE space of each buffer triangle subdivision must contain the FE space of its generating parent triangle.
3) For $H(curl)$ elements [7] [8], the FE space of each buffer triangle subdivision must include the gradients of

Manuscript received July 1, 2003.

The authors are with Lehrstuhl für Theoretische Elektrotechnik, Dept. of Electrical Engineering, Saarland University, Saarbrücken, D-66123, Germany (telephone (+49) (+681) 302-2441, e-mail: roman.edlinger@ieee.org).

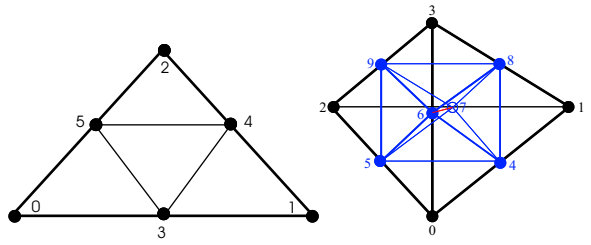


Fig. 2. a: Subdivision of triangle. b: Subdivision of tetrahedron.

all $H^1$ basis functions associated with the mid-nodes at the interface to the fine mesh region. In Fig. 1c, the FE space of the $T_{061}$ subdivision must include $\nabla N_3$.

Requirement 3 guarantees that the $H(curl)$ conforming FE space includes the gradients of all $H^1$ basis functions associated with the same discretization, as with conventional Whitney elements. The such constructed FE spaces inherits all essential properties of the underlying Whitney spaces [8], notably the exact sequence property in topologically simple domains. In the $H(curl)$ case, it is therefore still possible to apply a tree gauge [9].

## III. Restriction Operators

In order to construct above constraints, we need to express coarse mesh basis functions in terms of their fine mesh counterparts, which is accomplished by the corresponding restriction operator $R_f^c$. In the following, we write $n_i$ for $H^1$ nodal and $e_{ik}$ for $H(curl)$ edge basis functions and indicate the coarse and fine mesh levels by $c$ and $f$, respectively. Using the node numbering of Fig. 2, the coefficients of the restriction operator are obtained for triangles from

$$n_0^c = n_0^f + \tfrac{1}{2}(n_3^f + n_5^f), \tag{1}$$
$$e_{01}^c = \tfrac{1}{2}(e_{03}^f + e_{31}^f) + \tfrac{1}{4}(e_{34}^f + e_{54}^f + e_{53}^f), \tag{2}$$

and for tetrahedra from

$$n_0^c = n_0^f + \tfrac{1}{2}(n_4^f + n_5^f + n_6^f), \tag{3}$$
$$\begin{aligned} e_{01}^c = {} & \tfrac{1}{2}(e_{04}^f + e_{41}^f) + \tfrac{1}{4}(e_{57}^f + e_{68}^f) \\ & + \tfrac{1}{4}(e_{54}^f - e_{46}^f + e_{47}^f + e_{48}^f) + \tfrac{1}{4}e_{67}^f, \end{aligned} \tag{4}$$
$$\begin{aligned} e_{03}^c = {} & \tfrac{1}{2}(e_{06}^f + e_{63}^f) + \tfrac{1}{4}(e_{48}^f + e_{59}^f) \\ & + \tfrac{1}{4}(e_{46}^f + e_{56}^f + e_{68}^f + e_{69}^f). \end{aligned} \tag{5}$$

Note that, for tetrahedral edges, there are two different equations (4) (5) which depend on the location of the coarse mesh edge relative to the interior edge $E_{67}^f$.

## IV. Basic Refinement

In basic refinement, we keep all fine mesh basis functions in the subdivisions of buffer elements and apply restrictions (1)-(5) to impose the proper continuity conditions at the interface to the coarse mesh domain. Basic refinement is conceptually simple, and it is easy to verify that requirements 1 - 3 of Section II hold.

On the other hand, Fig. 1c shows that the number of extra edges introduced in the buffer region may be significant. For edge or higher order nodal elements, such edges generate extra variables in addition to those in the fine mesh region. In auto-adaptive methods, where we want to place degrees of freedom most selectively, the basic refinement method is therefore not the best choice.

## V. Advanced Refinement

For optimum computational efficiency, we want to add to the buffer elements only degrees of freedom that are absolutely necessary to maintain sufficient continuity across the interface to the fine mesh region. Since there are no interior variables in the first order $H^1$ case, we consider $H(curl)$ edge elements only.

### A. Two-dimensional case

Let the triangle of Fig. 2a be located in the buffer region with the fine mesh adjacent to edge $E_{01}$. In this case, we construct the FE space from the coarse mesh functions $e_{12}^c$ and $e_{20}^c$ plus two intermediate functions $e_{03}^i$, $e_{31}^i$. Since $e_{03}^i$, $e_{31}^i$ must have vanishing tangential components along edges $E_{12}$ and $E_{20}$, they are of the general form

$$e_{03}^i = e_{03}^f + \alpha_1 e_{34}^f + \beta_1 e_{54}^f + \gamma_1 e_{53}^f, \tag{6}$$
$$e_{31}^i = e_{31}^f + \gamma_2 e_{34}^f + \beta_2 e_{54}^f + \alpha_2 e_{53}^f, \tag{7}$$

where the coefficients $\alpha_1 \ldots \gamma_2$ are yet to be determined. For Requirement 2 to hold, the space spanned by $e_{03}^i$, $e_{31}^i$ must be able to represent the missing coarse mesh basis function $e_{01}^c$. Similarly, to meet Requirement 3, $e_{03}^i$, $e_{31}^i$ must be able to represent the mid-point gradient $\nabla n_3^f$,

$$\nabla n_3^f = e_{03}^f - e_{31}^f - e_{34}^f + e_{53}^f. \tag{8}$$

Equality along edge $E_{01}$ implies

$$e_{01}^c = \tfrac{1}{2}(e_{03}^i + e_{31}^i), \tag{9}$$
$$\nabla n_3^f = (e_{03}^i - e_{31}^i). \tag{10}$$

Next, we use the restriction operator (2) as well as the general forms (6) and (7) to express (9) and (10) in terms of fine mesh functions:

$$\begin{aligned} & \tfrac{1}{2}(e_{03}^f + e_{31}^f) + \tfrac{1}{4}(e_{34}^f + e_{54}^f + e_{53}^f) = \\ & \quad + \tfrac{1}{2}(e_{03}^f + \alpha_1 e_{34}^f + \beta_1 e_{54}^f + \gamma_1 e_{53}^f) \\ & \quad + \tfrac{1}{2}(e_{31}^f + \gamma_2 e_{34}^f + \beta_2 e_{54}^f + \alpha_2 e_{53}^f), \end{aligned} \tag{11}$$
$$\begin{aligned} & e_{03}^f - e_{31}^f - e_{34}^f + e_{53}^f = \\ & \quad + (e_{03}^f + \alpha_1 e_{34}^f + \beta_1 e_{54}^f + \gamma_1 e_{53}^f) \\ & \quad - (e_{31}^f + \gamma_2 e_{34}^f + \beta_2 e_{54}^f + \alpha_2 e_{53}^f). \end{aligned} \tag{12}$$

By comparing coefficients in (11) and (12), we arrive at

$$\alpha_1 + \gamma_2 = \tfrac{1}{2}, \quad \beta_1 + \beta_2 = \tfrac{1}{2}, \quad \gamma_1 + \alpha_2 = \tfrac{1}{2}, \tag{13}$$
$$\alpha_1 - \gamma_2 = -1 \quad \beta_1 - \beta_2 = 0 \quad \gamma_1 - \alpha_2 = 1, \tag{14}$$

yielding

$$\alpha_1 = \alpha_2 = -\tfrac{1}{4}, \quad \beta_1 = \beta_2 = \tfrac{1}{4}, \quad \gamma_1 = \gamma_2 = \tfrac{3}{4}. \tag{15}$$

Hence our final results read

$$e_{03}^i = e_{03}^f - \tfrac{1}{4}e_{34}^f + \tfrac{1}{4}e_{54}^f + \tfrac{3}{4}e_{53}^f, \tag{16}$$
$$e_{31}^i = e_{31}^f + \tfrac{3}{4}e_{34}^f + \tfrac{1}{4}e_{54}^f - \tfrac{1}{4}e_{53}^f. \tag{17}$$

### B. Three-dimensional case

In three dimensions, the subdivision of a buffer tetrahedron may share an edge or an entire face with elements in the fine mesh region.

In the following, we always refer to the tetrahedron of Fig. 2b. We first treat the case of a common edge, which is essentially the same as in two dimensions but requires some care with regard to edge $E_{03}$. Even though the representation (5) of the coarse mesh basis function $e^c_{03}$ does not involve any contributions from the interior edge $e^f_{67}$, the latter *must be included* in the general equations for the intermediate functions $e^i_{06}$ and $e^i_{63}$:

$$\begin{aligned} e^i_{06} &= e^f_{06} + (\alpha_1 e^f_{68} + \alpha_2 e^f_{69}) + (\beta_1 e^f_{48} + \beta_2 e^f_{59}) \\ &\quad + (\gamma_1 e^f_{46} + \gamma_2 e^f_{56}) + \delta_1 e^f_{67}, \qquad (18) \\ e^i_{63} &= e^f_{63} + (\gamma_3 e^f_{68} + \gamma_4 e^f_{69}) + (\beta_3 e^f_{48} + \beta_4 e^f_{59}) \\ &\quad + (\alpha_3 e^f_{46} + \alpha_4 e^f_{56}) + \delta_2 e^f_{67}. \qquad (19) \end{aligned}$$

By taking $e^i_{06}$ and $e^i_{63}$ at the boundaries $T_{013}$ and $T_{032}$, we conclude from our results for the two-dimensional case that

$$\alpha_1 = \alpha_2 = \alpha_3 = \alpha_4 = -\tfrac{1}{4}, \qquad (20)$$

$$\beta_1 = \beta_2 = \beta_3 = \beta_4 = \tfrac{1}{4}, \qquad (21)$$

$$\gamma_1 = \gamma_2 = \gamma_3 = \gamma_4 = \tfrac{3}{4}. \qquad (22)$$

Requirements 2 and 3, i.e. representability of the coarse mesh function $e^c_{03}$ as well as the mid-point gradient $\nabla n^f_6$,

$$\nabla n^f_6 = e^f_{06} - e^f_{63} + e^f_{56} + e^f_{46} - e^f_{68} - e^f_{69} - e^f_{67}, \qquad (23)$$

yield

$$\delta_1 + \delta_2 = 0, \qquad (24)$$

$$\delta_1 - \delta_2 = -1, \qquad (25)$$

so that we have

$$\delta_1 = -\tfrac{1}{2}, \qquad \delta_2 = +\tfrac{1}{2}. \qquad (26)$$

We omit details for $e^i_{04}$ and $e^i_{41}$ and just give the final results:

$$\begin{aligned} e^i_{06} &= e^f_{06} - \tfrac{1}{4}(e^f_{68} + e^f_{69}) + \tfrac{1}{4}(e^f_{48} + e^f_{59}) \\ &\quad + \tfrac{3}{4}(e^f_{46} + e^f_{56}) - \tfrac{1}{2} e^f_{67}, \qquad (27) \\ e^i_{63} &= e^f_{63} + \tfrac{3}{4}(e^f_{68} + e^f_{69}) + \tfrac{1}{4}(e^f_{48} + e^f_{59}) \\ &\quad - \tfrac{1}{4}(e^f_{46} + e^f_{56}) + \tfrac{1}{2} e^f_{67}, \qquad (28) \\ e^i_{04} &= e^f_{04} - \tfrac{1}{4}(e^f_{47} + e^f_{48}) + \tfrac{1}{4}(e^f_{57} + e^f_{68}) \\ &\quad + \tfrac{3}{4}(e^f_{54} - e^f_{46}) + \tfrac{1}{4} e^f_{67}, \qquad (29) \\ e^i_{41} &= e^f_{41} + \tfrac{3}{4}(e^f_{47} + e^f_{48}) + \tfrac{1}{4}(e^f_{57} + e^f_{68}) \\ &\quad - \tfrac{1}{4}(e^f_{54} - e^f_{46}) + \tfrac{1}{4} e^f_{67}. \qquad (30) \end{aligned}$$

In the case of a common triangle, say $T_{013}$, our strategy is quite simple: just transform basis functions associated with outer edges ($E_{01}$, $E_{12}$, $E_{20}$) as in the previous case and keep those associated with inner edges ($E_{48}$, $E_{68}$, $E_{64}$) unchanged. To see that this yields a valid method, recall that the such generated basis functions still span the same FE space as the fine grid functions over the subdivision of the triangle $T_{013}$.

All basis functions in the buffer region that are not associated with the interface to the fine mesh are reduced to coarse grid functions by means of the usual multigrid restriction operators (3)-(5).

## VI. Matrix Assembly

Equations (16) (17) and (27)-(30) describe generalized restriction operators $[R]$ which can be applied in a multigrid-like fashion. In our computer implementation, we first create a raw finite element matrix $[M]_{raw}$ which includes all hanging variables. To impose the proper interface conditions, we then transform $[M]_{raw}$ to a valid FE matrix $[M]_{valid}$ by a Galerkin-type operation:

$$[M]_{valid} = [R][M]_{raw}[R]^T, \qquad (31)$$

$$[R] = [R]^0_1 [R]^1_2 \cdots [R]^{i-1}_i, \qquad (32)$$

where $[R]^{i-1}_i$ refers to hanging variables at the $i$-th refinement level.

## VII. Numerical Validation

For our numerical tests, we have solved a number of microwave examples by the vector-scalar-potential method of [5], which enables us to test both $H^1$ and $H(curl)$ elements in a single computer run. Our first example is a dielectric obstacle within a rectangular waveguide as shown in Fig. 3. A view of the non-uniform mesh along the symmetry plane of the device is given in Fig. 4. Second, we consider the microwave patch antenna of Fig. 5. Our third example, a microstrip bandpass filter, is depicted in Fig. 6. Since our solutions for the basic or advanced refinement methods are almost identical, i.e. reflection coefficients differ in the fourth digit only, we do not give separate data. In all cases, our numerical solutions are in good agreement with reference data from the literature [10], [11], [12].

Table I gives a comparison of the basic and advanced methods for different levels of refinement. We present variable counts, non-zero entries in the FE matrix and LU-factorization, as well as iteration counts for a multigrid-preconditioned conjugate gradient (CG) type solver. In case of direct factorization, the public-domain package METIS [13] is used for matrix reordering. It can be seen that the advanced method is always superior in terms of variable count and memory consumption, and comparable or better regarding iteration counts. However, the differences become less pronounced when the mesh size is getting large. We attribute this to the fact that, in our experimental setup, hanging variables are created by simply assigning unequal refinement levels to adjacent material regions. For high resolution meshes, the vast majority of unknowns gets generated inside volumes of uniform refinement, and surface effects such as the differences between our refinement schemes become less visible. In auto-adaptive FE methods, refinement levels are expected to become far less uniform.

For the dielectric obstacle, we report one more experiment marked "wrong" in Table I. We have modified the intermediate $H(curl)$ basis functions (18) (19) such that the gradient inclusion condition, Requirement 3, is violated. Even though we do not see noticeable changes in the solution, the behavior of the iterative solver deteriorates significantly.

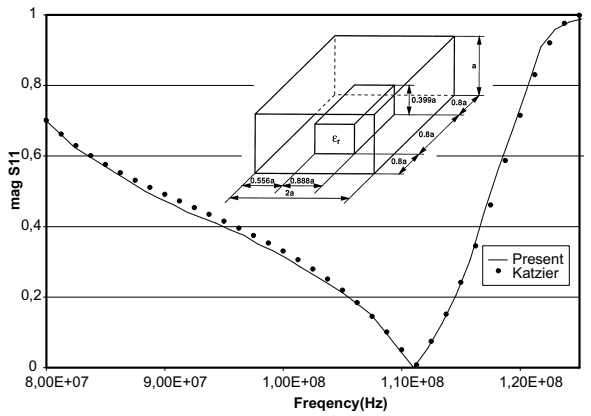


Fig. 3. Dielectric obstacle in rectangular waveguide: linear dimension $a = 1m$, relative permittivity $\varepsilon_r = 6$. Reference values taken from [10].

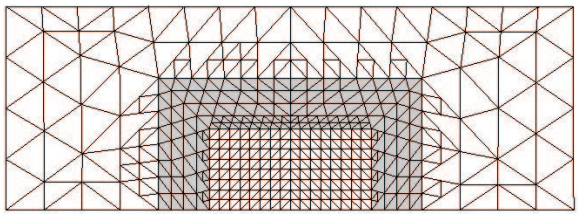

Fig. 4. Non-uniform mesh along symmetry plane of waveguide structure.

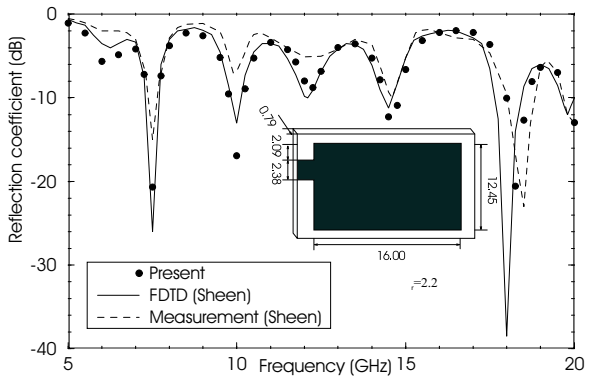


Fig. 5. Microwave patch antenna. All dimensions are in millimeter. Reference values taken from [11].

TABLE I
COMPARISON OF REFINEMENT METHODS

| Example | Method | Variables | Non-zeros FE Matrix | Non-zeros Factor. | CG-Iter. |
|---|---|---|---|---|---|
| Obstacle | Basic | 83323 | 1.17e6 | 3.4e7 | 12 |
| 2 1 0 | Advanced | 73775 | 1.06e6 | 2.8e7 | 12 |
| | Wrong | 73775 | 1.00e6 | 2.8e7 | 26 |
| Obstacle | Basic | 608157 | 8.77e6 | 5.56e8 | 20 |
| 3 2 1 | Advanced | 572189 | 8.32e6 | 4.98e8 | 20 |
| Patch | Basic | 9499 | 1.09e5 | 8.41e5 | 19 |
| 1 0 | Advanced | 8038 | 9.30e4 | 6.60e5 | 19 |
| Patch | Basic | 65074 | 8.54e5 | 1.49e7 | 36 |
| 2 1 | Advanced | 59419 | 7.89e5 | 1.31e7 | 35 |
| Patch | Basic | 478784 | 6.7e6 | 2.77e8 | 51 |
| 3 2 | Advanced | 456533 | 6.44e6 | 2.55e8 | 52 |
| Bandpass | Basic | 12231 | 1.14e5 | 6.8e5 | 46 |
| 1 0 | Advanced | 10643 | 9.80e4 | 5.73e5 | 35 |
| Bandpass | Basic | 83746 | 9.79e5 | 1.46e7 | 60 |
| 2 1 | Advanced | 77261 | 9.10e5 | 1.27e7 | 51 |
| Bandpass | Basic | 613909 | 8.08e6 | 2.87e8 | 82 |
| 3 2 | Advanced | 587769 | 7.79e6 | 2.71e8 | 73 |

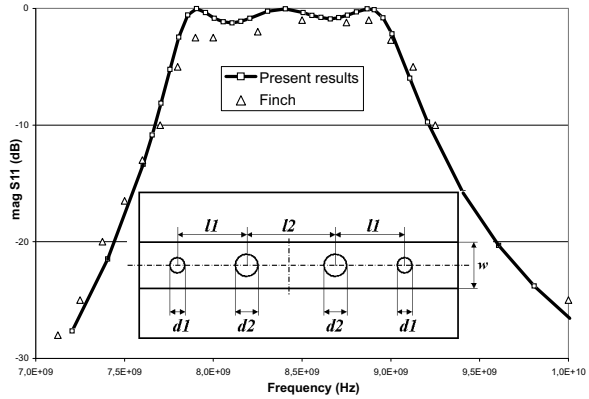


Fig. 6. Microstrip bandpass filter. $\epsilon_r$ = 2.43, d1 = 0.333mm, d2 = 0.9323mm, l1 = 10.42mm, l2 = 11.15mm, w = 3.79mm, substrate height = 0.49mm. Reference values taken from [12].

## VIII. CONCLUSION

Hanging variables provide an attractive way to construct perfectly nested hierarchies of finite elements of non-uniform refinement levels. In this paper, we have proposed an advanced refinement strategy, which is more efficient than a straightforward approach, in the sense that it keeps the number of variables and non-zero matrix entries at a minimum. The suggested method keeps all important properties of the underlying Whitney element spaces intact, and our numerical experiments have shown that it has no adverse effects on the numerical convergence characteristics of iterative solvers.

## REFERENCES

[1] V.V. Shaidurov, *Multigrid Methods for Finite Elements*, pp. 68-70, Dortrecht, The Netherlands: Kluwer Academic Publishers, 1995.

[2] J.P. Webb and S. McFee, "Nested Tetrahedral Finite Elements for $h$-Adaption," *IEEE Trans. Magn.*, vol. 33, pp. 1338-1341, 1999.

[3] F. Bornemann, B. Erdmann, R. Kornhuber, "Adaptive Multilevel Methods in Three Space Dimensions," *Report SC-92-14*, Konrad-Zuse-Zentrum für Informationstechnik, Berlin, Germany, 1992.

[4] U. Rüde, *Mathematical and Computational Techniques for Multilevel Adaptive Methods*, pp. 100-108, Philadelphia, PA: SIAM, 1993.

[5] V. Hill, O. Farle, and R. Dyczij-Edlinger, "A Stabilized Multi-Level Vector Finite Element Solver for Time-Harmonic EM Waves," *IEEE Trans. Magn.*, vol. 39, pp. 1203-1206, May 2003.

[6] P. Knabner and L. Angermann, *Numerik partieller Differentialgleichungen*, p. 175, Berlin, Germany: Springer-Verlag, 2000 (in German).

[7] D. Sun, Z. Cendes, "New vector finite elements for three-dimensional magnetic fields computations," *J. Appl. Phys.*, vol. 61, no. 8, pp. 3919-3921, April 1987.

[8] A. Bossavit, "A Rationale for Edge-Elements in 3-D Fields Computations," *IEEE Trans. Magn.*, vol. 24, pp. 74-79, Jan. 1988.

[9] R. Albanese and R. Rubinacci, "Solution of three dimensional eddy current problems by integral and differential methods," *IEEE Trans. Magn.*, vol. 24, pp. 98-101, 1988.

[10] H. Katzier, "Streuverhalten elektromagnetischer Wellen bei sprunghaften Übergängen geschirmter dielektrischer Leitungen," *AEÜ*, vol. 38, pp. 290-296, 1984 (in German).

[11] D.M. Sheen, S.M. Ali, M.D. Abouzahra, J.A. Kong, "Application of the Three-Dimensional Finite-Difference Time-Domain Method to the Analysis of Planar Microstrip Circuits," *IEEE Trans. Microwave Theory & Tech.*, vol. 38, pp. 849-857, 1990.

[12] K.L. Finch and N.G. Alexopoulos, "Shunt posts in microstrip transmission lines," *IEEE Trans. Microwave Theory & Tech.*, vol. 38, pp. 1585-1594, 1990.

[13] The METIS homepage at http://www-users.cs.umn.edu/˜karypis/metis.